View metadata, citation and similar papers at core.ac.uk

brought to you by CORE

provided by DSpace@MIT

The Astrophysical Journal, 832:114 (7pp), 2016 December 1 doi:10.3847/0004-637X/832/2/114

© 2016. The American Astronomical Society. All rights reserved.

SPT0346-52: NEGLIGIBLE AGN ACTIVITY IN A COMPACT, HYPER-STARBURST GALAXY AT $z = 5.7$

Jingzhe Ma[1], Anthony. H. Gonzalez[1], J. D. Vieira[2], M. Aravena[3], M. L. N. Ashby[4], M. Béthermin[5], M. S. Bothwell[6], W. N. Brandt[7,8,9], C. de Breuck[5], J. E. Carlstrom[10], S. C. Chapman[11], B. Gullberg[5], Y. Hezaveh[12,18], K. Litke[13], M. Malkan[14], D. P. Marrone[13], M. McDonald[15], E. J. Murphy[16], J. S. Spilker[13], J. Sreevani[2], A. A. Stark[4], M. Strandet[17], and S. X. Wang[9]

[1] Department of Astronomy, University of Florida, Gainesville, FL 32611, USA; jingzhema@ufl.edu
[2] Department of Astronomy and Department of Physics, University of Illinois, 1002 West Green St., Urbana, IL 61801, USA
[3] Núcleo de Astronomía, Facultad de Ingeniería, Universidad Diego Portales, Av. Ejército 441, Santiago, Chile
[4] Harvard-Smithsonian Center for Astrophysics, 60 Garden Street, Cambridge, MA 02138, USA
[5] European Southern Observatory, Karl Schwarzschild Straße 2, D-85748 Garching, Germany
[6] Cavendish Laboratory, University of Cambridge, JJ Thompson Ave, Cambridge CB3 0HA, UK
[7] Institute for Gravitation and the Cosmos, The Pennsylvania State University, University Park, PA 16802, USA
[8] Department of Physics, The Pennsylvania State University, University Park, PA 16802, USA
[9] Department of Astronomy and Astrophysics, The Pennsylvania State University, University Park, PA 16802, USA
[10] Kavli Institute for Cosmological Physics, University of Chicago, 5640 South Ellis Avenue, Chicago, IL 60637, USA
[11] Dalhousie University, Halifax, Nova Scotia, Canada
[12] Kavli Institute for Particle Astrophysics and Cosmology, Stanford University, Stanford, CA 94305, USA
[13] Steward Observatory, University of Arizona, 933 North Cherry Avenue, Tucson, AZ 85721, USA
[14] Department of Physics and Astronomy, University of California, Los Angeles, CA 90095-1547, USA
[15] Kavli Institute for Astrophysics and Space Research, Massachusetts Institute of Technology, 37-582C, Cambridge, MA 02139, USA
[16] National Radio Astronomy Observatory, 520 Edgemont Road, Charlottesville, VA 22903, USA
[17] Max-Planck-Institut für Radioastronomie, Auf dem Hügel 69 D-53121 Bonn, Germany

Received 2016 May 5; revised 2016 September 20; accepted 2016 September 27; published 2016 November 22

ABSTRACT

We present *Chandra* ACIS-S and Australia Telescope Compact Array (ATCA) radio continuum observations of the strongly lensed dusty, star-forming galaxy SPT-S J034640-5204.9 (hereafter SPT0346-52) at $z = 5.656$. This galaxy has also been observed with ALMA, *HST*, *Spitzer*, *Herschel*, Atacama Pathfinder EXperiment, and the Very Large Telescope. Previous observations indicate that if the infrared (IR) emission is driven by star formation, then the inferred lensing-corrected star formation rate (SFR) ($\sim 4500\,M_\odot\,\mathrm{yr}^{-1}$) and SFR surface density Σ_{SFR} ($\sim 2000\,M_\odot\ \mathrm{yr}^{-1}\ \mathrm{kpc}^{-2}$) are both exceptionally high. It remained unclear from the previous data, however, whether a central active galactic nucleus (AGN) contributes appreciably to the IR luminosity. The *Chandra* upper limit shows that SPT0346-52 is consistent with being star formation dominated in the X-ray, and any AGN contribution to the IR emission is negligible. The ATCA radio continuum upper limits are also consistent with the FIR-to-radio correlation for star-forming galaxies with no indication of an additional AGN contribution. The observed prodigious intrinsic IR luminosity of $(3.6 \pm 0.3) \times 10^{13}\,L_\odot$ originates almost solely from vigorous star formation activity. With an intrinsic source size of 0.61 ± 0.03 kpc, SPT0346-52 is confirmed to have one of the highest Σ_{SFR} of any known galaxy. This high Σ_{SFR}, which approaches the Eddington limit for a radiation pressure supported starburst, may be explained by a combination of very high star formation efficiency and gas fraction.

Key words: galaxies: high-redshift

1. INTRODUCTION

A population of gravitationally lensed dusty star-forming galaxies (DSFGs) has been discovered by the South Pole Telescope (SPT) survey (Vieira et al. 2010) and facilitated our understanding of the stellar, gas, and dust content of the high-redshift universe. One of the sources stands out as the most extraordinary discovered so far in the 2500 deg^2 survey: SPT-S J034640-5204.9 (hereafter SPT0346-52) at $z = 5.656$, among the highest-redshift DSFGs known. It has been the focus of a multi-wavelength observational campaign with *HST*, *Spitzer*, *Herschel*, the Atacama Large Millimeter/submillimeter Array (ALMA), the Atacama Pathfinder EXperiment (APEX), and the Very Large Telescope (VLT).

Our lens model obtained from ALMA 870 μm imaging shows that SPT0346-52 is magnified by the foreground lensing galaxy (at $z \sim 1.1$) a factor of 5.6 ± 0.1 with an intrinsic 870 μm flux of 19.6 ± 0.5 mJy, and has an intrinsic size of $R_{\mathrm{eff}} = 0.61 \pm 0.03$ kpc (R_{eff} being half-light radius; Hezaveh et al. 2013; Spilker et al. 2016). Multi-band spectral energy distribution (SED) fitting gives an intrinsic infrared (IR; 8–1000 μm) luminosity L_{IR} of $(3.6 \pm 0.3) \times 10^{13}\,L_\odot$ and a star formation rate (SFR) of $4500 \pm 1000\,M_\odot\,\mathrm{yr}^{-1}$ (Ma et al. 2015). Given its size, SPT0346-52 turns out to have one of the highest IR luminosity surface densities and SFR surface densities Σ_{SFR} of any known galaxy (Hezaveh et al. 2013; Spilker et al. 2015, 2016). The central question is whether this high-luminosity surface density arises solely from intense star formation or if there is an obscured active galactic nucleus (AGN).

The dust temperature of SPT0346-52, 52.4 ± 2.2 K (Gullberg et al. 2015), is higher than that of typical DSFGs and reaches into the territory of AGN-dominated sources (Figure 1). SPT0346-52 has an $L_{[\mathrm{C\,II}]}/L_{\mathrm{FIR}}$ ratio consistent with FIR-luminous quasars at $z \sim 6$ and also shows an $L_{[\mathrm{C\,II}]}$ deficit relative to L_{FIR} and $L_{\mathrm{CO}(1-0)}$, which has been observed in AGN-dominated sources (Stacey et al. 2010; Sargsyan et al. 2014; Gullberg et al. 2015). It shows strong H_2O

[18] Hubble Fellow.

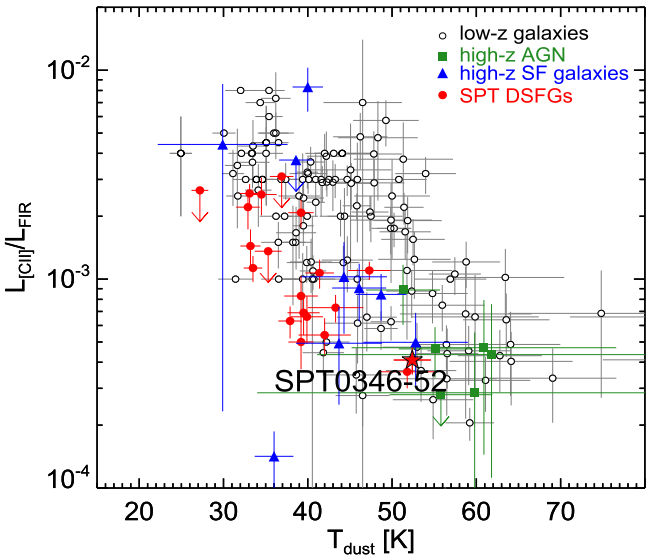

Figure 1. $L_{[\mathrm{C\ II}]}/L_{\mathrm{FIR}}$ vs. T_{dust}. The red circles are SPT DSFGs. The low-z and high-z samples are compiled by Gullberg et al. (2015; see references therein). SPT0346-52 (red star) lies in the region surrounded by AGN-dominated galaxies. This diagnostic provided the motivation to search for X-ray signatures of an AGN in this extreme source.

emission lines (Weiß et al. 2013) similar to that of the strongly lensed quasars H1413+1143 and APM 08279+5255 (Bradford et al. 2011). SPT0346-52 is also optically obscured and does not show any indications of type-1 or type-2 AGN in deep VLT optical spectroscopy (Hezaveh et al. 2013).

DSFGs are in a unique phase of galaxy formation and evolution where the assembly of the stellar and super massive black hole (SMBH) masses are believed to be closely coupled (Alexander & Hickox 2012). To test if SPT0346-52 hosts an AGN and determine whether it is star formation dominated or AGN dominated, we resort to *Chandra*. Hard X-ray emission (rest-frame energies >2 keV) is the best indicator of AGN activity. These high-energy photons can penetrate through heavy obscuration, revealing the signature of the accreting black hole. A significant fraction of X-ray detected DSFGs have been found to be AGN dominated in the X-ray, while some are powered by pure star formation (e.g., Laird et al. 2010; Georgantopoulos et al. 2011; Johnson et al. 2013). X-ray observations of the well-studied DSFG samples from the ALMA LABOCA E-CDF-S Submillimeter Survey (ALESS; Wang et al. 2013b) reveal that 17% of DSFGs appear to host an AGN. We here compare SPT0346-52 with these DSFGs and starbursts and quasars in the literature to understand the nature of the most extraordinary source found so far in the SPT survey.

In addition to X-ray, radio also can be used to distinguish star-forming galaxies from AGN. Radio continuum emission from galaxies arises due to both thermal and non-thermal processes in massive star formation. These same massive stars also provide the primary sources of dust heating in the interstellar medium, and the FIR emission is primarily due to the re-emitted starlight by dust. Star-forming galaxies that are not radio-loud AGN are observed to follow a tight FIR-to-radio correlation that holds over five orders of magnitude in galaxy luminosity (e.g., Yun et al. 2001). In contrast, radio-loud AGN will exhibit elevated radio emission above this relation (e.g., Yun et al. 2001; Condon et al. 2002). We utilize the Australia Telescope Compact Array (ATCA) to probe the radio continuum emission of SPT0346-52 to examine whether or not it is consistent with the FIR-to-radio correlation.

Table 1
Multi-wavelength Observed Flux Densities in mJy

Telescope	Wavelength	SPT-S J034640-5204.9
HST/WFC3	1.1 μm	$<3.8 \times 10^{-4}$
HST/WFC3	1.6 μm	$<9.1 \times 10^{-4}$
Spitzer/IRAC	3.6 μm	<0.0024
Spitzer/IRAC	4.5 μm	<0.0036
Herschel/PACS	100 μm	<6
Herschel/PACS	160 μm	33 ± 9
Herschel/SPIRE	250 μm	122 ± 11
Herschel/SPIRE	350 μm	181 ± 14
Herschel/SPIRE	500 μm	204 ± 15
APEX/LABOCA	870 μm	131 ± 8
SPT	1.4 mm	46.0 ± 6.8
SPT	2.0 mm	11.6 ± 1.3
ATCA	5.5 cm	<0.114
ATCA	14.3 cm	<0.213

Note. For the non-detections, the flux upper limits are given at 3σ. To derive the intrinsic flux densities, we divide the observed values by $\mu = 5.6 \pm 0.1$.

In this paper, we present the results from X-ray observations with the *Chandra* Observatory and radio continuum observations with ATCA to constrain the AGN activity, in combination with our existing multi-wavelength data. The Galactic column density toward SPT0346-52 is $N_{\mathrm{H}} = 1.8 \times 10^{20}\,\mathrm{cm}^{-2}$. We assume a ΛCDM cosmology with $H_0 = 69.3\,\mathrm{km\,s^{-1}\,Mpc^{-1}}$, $\Omega_m = 0.286$, and $\Omega_\Lambda = 0.713$ (WMAP9; Hinshaw et al. 2013). We adopt the definition of L_{IR} to be integrated over rest-frame 8–1000 μm and L_{FIR} integrated over rest-frame 42.5–122.5 μm. We assume a Chabrier (2003) initial mass function (IMF) throughout the paper.

2. OBSERVATIONS

We present the new *Chandra* X-ray and ATCA radio continuum data for SPT0346-52 in this section. Previous near-IR to far-IR photometric data are summarized in Table 1.

2.1. Chandra X-ray Data

SPT0346-52 was observed with the Advanced CCD Imaging Spectrometer (ACIS; Garmire et al. 2003) on board *Chandra* on 2015 July 29. The source was placed at the aim point of the back-illuminated ACIS-S3 chip. The data were taken in Very Faint mode and were initially processed by the *Chandra* X-ray Center (CXC) using software version 10.4.1 and CalDB version 4.6.8.

We reprocessed the data with the *Chandra* Interactive Analysis of Observations (CIAO; version 4.7) tool *chandra_repro*. All of the bad pixels were removed and the standard grade (0, 2, 3, 4, 6), status, and good-time filters were applied. The net exposure time for the observation is 49.52 ks. We performed energy filtering on events into three *Chandra* bands: the soft (SB; 0.5–2.0 keV), hard (HB; 2–8 keV), and full (FB; 0.5–8.0 keV) bands. The soft and hard bands probe rest-frame energies 3.3–13.3 keV and 13.3–53.2 keV for $z = 5.656$, respectively. No detectable X-ray emission is expected from the foreground lens. Existing optical and radio data show no evidence for an AGN in the lens. Moreover, the foreground lens is an elliptical galaxy (based upon the light profile fitting

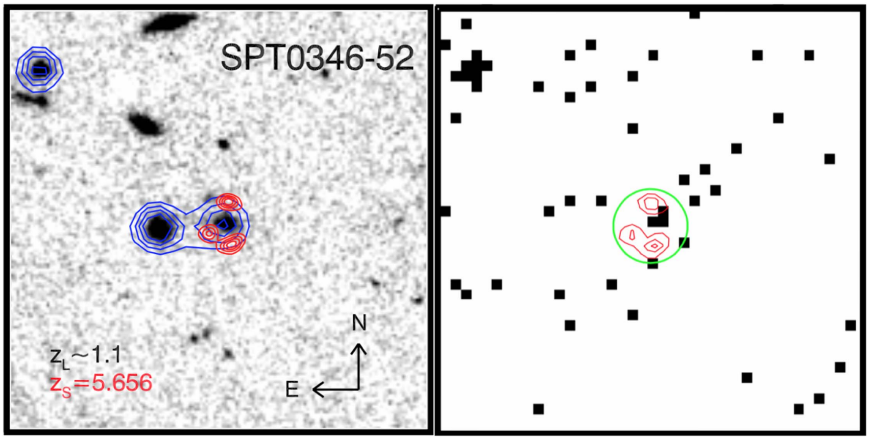

Figure 2. Left: 20″ × 20″ cutouts of SPT0346-52 showing the *HST*/WFC3 (gray), *Spitzer*/IRAC (blue contours), and ALMA band 7 (red contours) data. Right: *Chandra* 0.5–8 keV full-band data. The green circle shows the source extraction aperture enclosing the ALMA contours (red). The energies of the three photons are 1.284 (upper right), 2.585 (lower left), and 2.009 (lower right) keV.

Table 2
Chandra X-Ray Properties of SPT0346-52

Source Name	Redshift	Exptime (ks)	Full Band (count)	Background (count)	Full-band Flux (3σ) ($\times 10^{-15}$ erg cm^{-2} s^{-1})		Full-band Luminosity (3σ) ($\times 10^{44}$ erg s^{-1})	
					$f_{0.5-8\ \mathrm{keV}}$	$f_{0.5-8\ \mathrm{keV,unabs}}$	$L_{0.5-8\ \mathrm{keV}}$	$L_{0.5-8\ \mathrm{keV,unabs}}$
SPT0346-52	5.656	49.52	3.19	0.81	<1.07	<1.36	<1.20	<3.23

by Ma et al. 2015), and thus should also have negligible X-ray emission from star formation (more than three orders of magnitude below the detection threshold).

We matched the source to the position of ALMA (Figure 2) and used a source extraction radius of 1.″75 enclosing all of the lensed images, which is ∼1.3 times the 90% encircled-energy aperture radius (at 0.′3 off-axis angle). The aperture was chosen such that it is large enough to enclose the ALMA contours without including too much background. The background counts were estimated by placing 78 circular apertures with the same size at random positions in the field. We only detected 3.19 net source counts in the full band (0.73 in the SB and 2.47 in the HB). Due to the low count level, we utilize the tool *aprates* in the *srcflux* script in CIAO to place a proper upper limit on the X-ray flux. This tool employs Bayesian statistics to compute the background-marginalized posterior probability distribution for source counts/flux. The posterior distribution can be used to determine flux value and confidence intervals or upper limits. The resultant FB flux is consistent with a non-detection with a 3σ upper limit of 6.0×10^{-15} erg cm^{-2} s^{-1}. We derive the rest-frame 0.5–8 keV apparent luminosity $L_{0.5-8\ \mathrm{keV}}$ (without absorption correction) using the following equation:

$$L_{0.5-8\ \mathrm{keV}} = 4\pi d_L^2 f_{0.5-8\ \mathrm{keV}} (1+z)^{\Gamma_{\mathrm{eff}}-2}, \quad (1)$$

where d_L is the luminosity distance at $z = 5.656$ and Γ is the effective power-law photon index. In principle, the photon index can be derived from the hardness ratio, which is the ratio of the photon count rates in the HB and the SB. However, we cannot derive a reliable hardness ratio based on the upper limits in both bands. Instead, Γ_{eff} is fixed to 1.4 following Xue et al. (2011) and Wang et al. (2013b).

We then derive the rest-frame 0.5–8 keV absorption-corrected luminosity $L_{0.5-8\ \mathrm{keV,unabs}}$ by replacing Γ_{eff} with intrinsic photon index Γ_{int} and $f_{0.5-8\ \mathrm{keV}}$ with unabsorbed flux $f_{0.5-8\ \mathrm{keV,unabs}}$ in Equation (1). We assume $\Gamma_{\mathrm{int}} = 1.8$, a typical value for AGN. The unabsorbed flux is estimated using the tool *modelflux* within the *srcflux* script. We run simulations adopting Sherpa (Freeman et al. 2001) models *xspowerlaw* × *xszphabs* × *xsphabs* with fixed $\Gamma = 1.8$ for the power-law model and hydrogen column density N_{H} for the (intrinsic and Galactic) absorption models. We scale the measured 3σ upper limit on the flux by a fractional correction for absorption based on the typical intrinsic N_{H} (2.3×10^{23} cm^{-2}) from the ALESS SMG sample (Wang et al. 2013b). The absorption-corrected 3σ upper limit is $f_{0.5-8\ \mathrm{keV,unabs}} < 7.6 \times 10^{-15}$ erg cm^{-2} s^{-1}. Since SPT0346-52 is gravitationally lensed, we further correct the X-ray flux and luminosity for lensing magnification assuming there is no differential magnification between the FIR (i.e., ALMA) and the X-ray emission (Hezaveh et al. 2012). The magnification-corrected FB flux and luminosity upper limits are listed in Table 2.

2.2. ATCA Radio Data

SPT0346-52 was observed with ATCA for 3960 s at 5.5 and 9.0 GHz and 4068 s at 2.1 GHz on 2012 January 25 in the 6A array configuration using the CABB in the 1M-0.5k mode. The data was reduced in the same manner as in Aravena et al. (2013). The resultant synthesized beam sizes are 7.″7 × 5.″2 at 2.1 GHz, 3.″3 × 2.″2 at 5.5 GHz, and 2.″1 × 1.″3 at 9.0 GHz. The continuum was not detected in any band and we place 3σ upper limits (i.e., 3× rms noise values calculated within a 1′ region around the source position) of 0.213 mJy at 2.1 GHz, 0.114 mJy at 5.5 GHz, and 0.138 mJy at 9.0 GHz on the radio emission from the source.

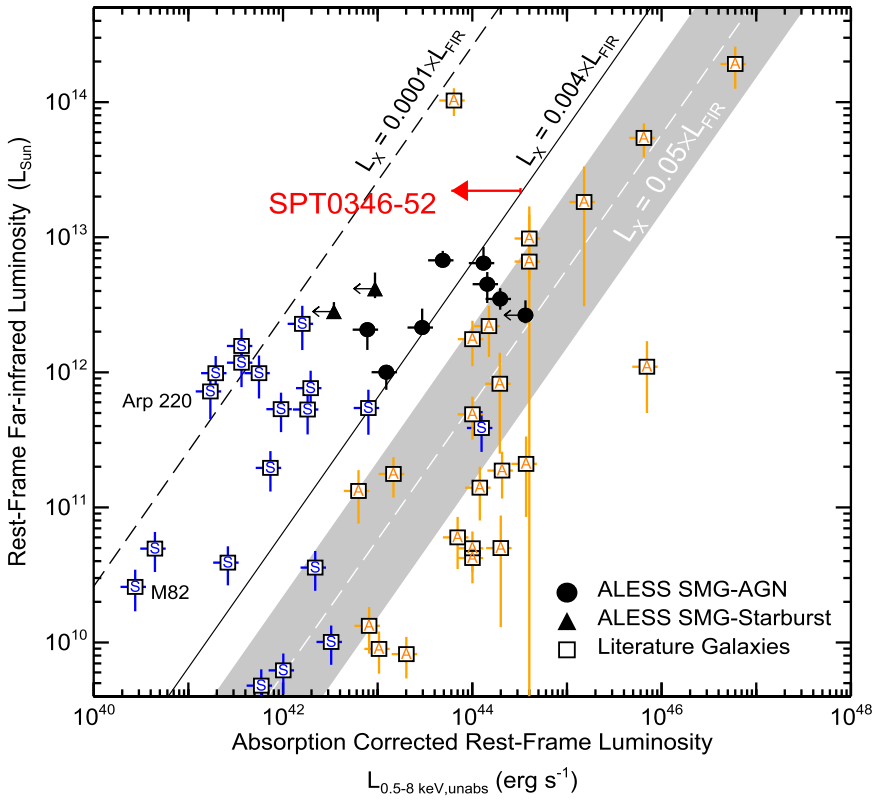

Figure 3. L_{FIR} vs. L_X for SMGs and literature galaxies. SPT0346-52 is the red arrow representing the 3σ upper limit on the absorption-corrected L_X. We have corrected L_{FIR} and L_X for lensing magnification. We show the ALESS SMGs from Wang et al. (2013b). The X-ray detected SMGs are marked as starburst-classified SMGs and AGN-classified SMGs. The dividing line between star formation dominated and AGN dominated appears to be $L_X = 0.004 \times L_{FIR}$, which is the median ratio of SCUBA SMGs found by Alexander et al. (2005). The squares are literature galaxies that are classified as star-formation dominated (labeled with blue "S") or AGN dominated (labeled with orange "A"). These data points are compiled by Alexander et al. (2005; see references therein) and we have re-fit the FIR photometry in a consistent manner as described in Gullberg et al. (2015). We assume 30% error on L_X for the literature galaxies. The dashed white line and the gray region represent the fiducial L_{FIR} vs. L_X relation and its standard deviation for the quasars in Elvis et al. (1994). The L_X-to-L_{FIR} ratio for pure starbursting systems (black dashed line) is about 2 orders of magnitude lower.

3. DISCUSSION

3.1. Observational/Empirical View

We place SPT0346-52 on the L_{FIR}–L_X plane (Figure 3) in the context of X-ray quasars and starburst galaxies. There, we compare it with other SMGs that are identified as SMG–AGN or SMG-starbursts to determine if it is star formation dominated or AGN dominated. As shown in Figure 3, the starburst galaxies (squares labeled with "S") from the literature occupy different locations than AGN-dominated galaxies (squares labeled with "A") and quasars (dashed line and the gray region). The well-studied unobscured quasars of Elvis et al. (1994) provide the fiducial X-ray to FIR luminosity ratios (the median ratio is $L_X/L_{FIR} = 0.05$ and the gray region indicates the standard deviation) for AGN-dominated sources. The luminosity ratio for pure starburst galaxies is about two orders of magnitude lower.

For SMGs, which may involve the co-evolution of SMBHs and the host galaxies, a heterogeneous population has been observed. The dividing line between starbursts and AGN is typically taken to be $L_X/L_{FIR} \sim 0.004$ (Alexander et al. 2005). The extensively studied ALESS SMGs from Wang et al. (2013b) are consistent with this notion. The X-ray to FIR ratio upper limit for SPT0346-52 is 0.0038, slightly leftward of the dividing line, which indicates that it is consistent with being starburst dominated in the X-ray. One caveat is that if the absorption for SPT0346-52 is exceptionally high, the X-ray upper limit could be weakened. For example, if N_H is 4 times higher (the highest N_H for ALESS SMGs) than what we adopted, the upper limit will be 1.3 times higher, which would move the limit slightly to the right of the dividing line between starbursts and AGN in Figure 3. For this reason, we also cannot exclude Compton-thick AGN by L_{FIR}–L_X alone (e.g., Murphy et al. 2009). The second potential caveat is AGN X-ray variability. Using the relation between X-ray luminosity and variability found by Lanzuisi et al. (2014), the fractional variability of SPT0346-52 is expected to be 30%. A third potential caveat is the possibility of differential magnification between the star formation region and the AGN (e.g., Hezaveh et al. 2012). We have assumed a constant magnification of $\mu = 5.6$. It could be that the star formation region is more magnified than the AGN. The maximum difference in magnification between components of this galaxy found by Spilker et al. (2015) is $\Delta\mu \sim 2$, which would move the red upper limit in Figure 3 by the same amount. However, without a robust X-ray detection and resolved X-ray image of the system, it is impossible to say any more.

If we adopt $L_X/L_{FIR} = 0.05$ for typical quasars and take the ratio $(L_X/L_{FIR})_{SPT0346\text{-}52}/(L_X/L_{FIR})_{quasars}$ following Alexander et al. (2005), the AGN fractional contribution to the FIR luminosity is estimated to be at most 8%. We note that an AGN in SPT0346-52 would be fainter than the quasars studied by Elvis et al. (1994), and that Seyfert 1 galaxies tend to be relatively more X-ray luminous than quasars. Using the

extensive Seyfert observations of Rush et al. (1996b) would shift the gray band in Figure 3 (and AGN/starburst boundary) to the right by a factor of a few. This would mean that the FIR contribution of any AGN in SPT0346-52 would be even smaller than our upper limit of 8%. Although we cannot completely rule out the presence of an AGN in the system, it is certainly the star formation that is dominating the FIR emission, which is confirmed by fitting SEDs including an AGN component in Section 3.2.

3.2. Constraining AGN Fraction Through SED Fitting

We previously performed SED fitting on SPT0346-52 with CIGALE FORTRAN assuming no AGN contribution in the IR (Ma et al. 2015), which is consistent with the NIR photometric upper limits and FIR detections. Now we employ CIGALE PYTHON (Roehlly et al. 2014), which includes up-to-date star formation history models, stellar population synthesis models, IR re-emission models, and AGN templates, to constrain the potential AGN contribution in the IR. The photometric data points used in the SED fitting are listed in Table 1. We adopt a Chabrier (2003) IMF and the Bruzual & Charlot (2003) stellar population synthesis models. For star formation history, we assume a delayed-τ model, which rises at early ages and then declines exponentially. This form of star formation history is generally expected for especially high-redshift galaxies (Pacifici et al. 2013; Simha et al. 2014; da Cunha et al. 2015). We use a combination of Dale et al. (2014) IR models accounting for the dust emission from the stellar component and Fritz et al. (2006) AGN templates. The Fritz et al. (2006) AGN models take into account two emission components associated with the AGN: a power law from the central source and the thermal and scattering dust-torus emission. The relative normalization of these components is handled through a parameter, fracAGN, which is the fractional contribution of the AGN to the total IR luminosity ($L_{\rm IR,total} = L_{\rm Starburst} + L_{\rm AGN}$). The model curve is also extended to radio wavelengths. The extension relies on the well-established FIR-to-radio correlation for star-forming galaxies. CIGALE does not include synchrotron emission from AGN.

A pure starburst SED remains the best-fit SED (i.e., with the minimal reduced χ^2), constrained by all of the photometric detections and upper limits from NIR to radio wavelengths (Figure 4). Parameters are analyzed under a Bayesian approach generating a posterior probability distribution function. The SED fitting failed to tightly constrain fracAGN given the lack of mid-IR photometric points (which differentiate between AGN and star-forming galaxies) and the loose constraint from the NIR. The posterior probability distribution suggests that the AGN component contributes at most ~20% to the total IR luminosity, with the highest probability being assigned to a contribution of 0%–5%. This is consistent with the estimation from the $L_{\rm X}/L_{\rm FIR}$ ratio in Section 3.1. The model SED with the maximum 20% AGN fraction is also plotted in Figure 4, which is inconsistent with the 100 μm *Herschel*/PACS upper limit.

The ATCA radio continuum upper limits at 2.1 and 5.5 GHz are consistent with the FIR-to-radio correlation for star-forming galaxies. The radio part of the SED for radio-loud AGN would be at least a factor of ~2 higher (e.g., Rush et al. 1996a, 1996b; Morić et al. 2010).

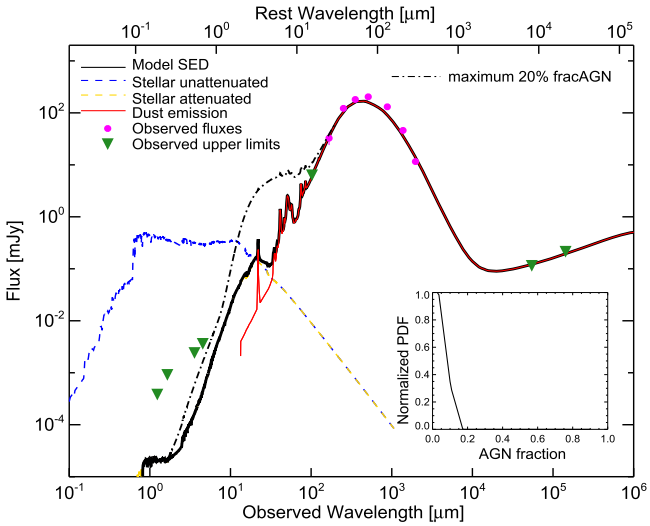

Figure 4. Best-fit SED (black) from CIGALE PYTHON. Different components are color-coded. The data points from left to right are *HST*/WFC3 F110W+F160W, *Spitzer*/IRAC 3.6 μm + 4.5 μm, *Herschel*/PACS 100 μm + 160 μm, *Herschel*/SPIRE 250 μm + 350 μm + 500 μm, APEX/LABOCA 870 μm, SPT 1.4 mm + 2.0 mm, and ATCA 5.5 GHz + 2.1 GHz. We do not include the ATCA 9.0 GHz upper limit, which is less constraining, because the source may be resolved at this frequency. The inset plot shows the normalized probability distribution function of the AGN fraction in the total IR luminosity. The AGN most probably contributes less than 5%. The dash–dotted line is the model curve with the maximum 20% AGN contribution to the IR. In this model, the AGN contribution does not extend to the radio part of the SED.

3.3. Theoretical Expectations

We have provided evidence that SPT0346-52 is star formation dominated in the IR. Since our SFR is mainly constrained by the FIR photometric data, $L_{\rm IR}$ being almost all from star formation suggests that the inferred SFR reflects the true SFR. We examine whether this observed high SFR can be physically explained in the framework of "maximum" starbursts (Elmegreen 1999) where a substantial fraction ϵ of available gas is consumed to make stars. Following Tacconi et al. (2006), the maximum ("Schmidt-law") SFR can be written as

$$\mathrm{SFR}_{\rm max} = \frac{\epsilon f_g M_{\rm tot}}{t_{\rm dyn}} = 630\left(\frac{\epsilon}{0.1}\right)\left(\frac{f_g}{0.4}\right)\left(\frac{v_c}{400}\right)^3 (M_\odot\ \mathrm{yr}^{-1}), \quad (2)$$

where Elmegreen (1999) defines ϵ as the star formation efficiency, f_g is the gas fraction, $M_{\rm tot}$ is the total (dynamical) mass of the system, $t_{\rm dyn}$ is the dynamical time, and v_c is the circular velocity in $\mathrm{km\,s^{-1}}$. We use the definition in Tacconi et al. (2006), $v_c = 0.67 \times v_{\rm FWHM} = 410\ \mathrm{km\,s^{-1}}$ ($v_{\rm FWHM} = 613 \pm 30\ \mathrm{km\,s^{-1}}$ measured from the low-J CO(2-1) line; Aravena et al. 2016). Assuming a gas fraction of 0.3–0.8, we utilize the observed SFR of $3600 \pm 300\ M_\odot\ \mathrm{yr}^{-1}$ to[19] derive ϵ, which turns out to be in the range of 0.3–0.7. This range is higher than the typical star formation efficiency (0.15–0.2) observed in DSFGs (Tacconi et al. 2006).

[19] Here we adopt the SFR converted directly from $L_{\rm IR}$ using the Kennicutt (1998) conversion factor assuming a Chabrier (2003) IMF where $\mathrm{SFR} = 1.0 \times 10^{-10}\ L_{\rm IR}\ (L_\odot)$.

We further examine the SFR surface density $\Sigma_{\rm SFR_{max}}$ expected from this framework;

$$\Sigma_{\rm SFR_{max}} = \frac{\rm SFR_{max}}{\pi R^2} = 43\left(\frac{\epsilon}{0.1}\right)\left(\frac{f_g}{0.4}\right)\left(\frac{\Sigma_{\rm tot}}{5000}\right)\left(\frac{R}{2}\right)^{-1}(M_\odot\ {\rm yr}^{-1}\,{\rm kpc}^{-2}), \quad (3)$$

where $\Sigma_{\rm tot}$ is the total (dynamical) mass density within radius R, in units of $M_\odot\,{\rm pc}^{-2}$. For SPT0346-52, $R = 1.8 \pm 0.2$ kpc and $M_{\rm tot} = (1.5 \pm 0.2) \times 10^{11}\,M_\odot$, derived in a spatially resolved CO imaging study by Spilker et al. (2015). The observed $\Sigma_{\rm SFR} = 1540 \pm 130\,M_\odot\ {\rm yr}^{-1}\ {\rm kpc}^{-2}$, in[20] which the dust emission (i.e., the stellar emission reprocessed by dust) is distributed in a compact area with an effective radius of 0.61 ± 0.03 kpc, surpasses the theoretical $\Sigma_{\rm SFR_{max}}$ by at least a factor of ~2. It is one of the highest star-formation densities of any known galaxy in the universe (Rujopakarn et al. 2011; Diamond-Stanic et al. 2012), although the nuclei of Arp 220 have $\Sigma_{\rm SFR} \sim 10^4\,M_\odot\ {\rm yr}^{-1}\ {\rm kpc}^{-2}$ (Barcos-Muñoz et al. 2015). Figure 6 shows how SPT0346-52 compares in SFR surface density to other starburst galaxies (black) and starbursts found in quasar host galaxies (green) at $z > 3$ in the literature. SPT0346-52 has an order of magnitude higher SFR than most other sources that lie within a factor of a few in star-formation surface density. SPT0346-52 stands out as the most extreme source at high redshift.

If the starburst is supported by radiation pressure on dust grains in a disk, $L_{\rm IR}$ is consistent with the Eddington-limited luminosity, but the SFR surface density is above the $\sim 1000\,M_\odot\ {\rm yr}^{-1}\ {\rm kpc}^{-2}$ theoretical limit by Thompson et al. (2005). The Eddington limit depends upon opacity, and the observed SFR for SPT0346-52 lies in between the $\rm SFR_{max,thin}$ for the optically thin limit and $\rm SFR_{max,thick}$ for the optically thick limit from Younger et al. (2008). The observed brightness temperature (~50 K) is comparable to the dust temperature, which suggests that the gas may be approaching the optically thick regime (Murray et al. 2005; Younger et al. 2008). Thus, the star formation activity in this source, while very vigorous, may still be sub-Eddington. It is natural to suspect that the radiation pressure would drive outflows of cold dusty gas, which have been commonly observed from starbursting galaxies including ultra-luminous IR galaxies (e.g., Martin 2005; Spoon et al. 2013; Veilleux et al. 2013).

3.4. Possible Explanations for the $\Sigma_{\rm SFR}$

Figure 5 demonstrates the allowed ϵ and $f_{\rm gas}$ in the theoretical framework of "maximum starbursts." This observed extremely high $\Sigma_{\rm SFR}$ may be explained by an especially high star-formation efficiency ($\epsilon > 0.4$) relative to what has been observed in DSFGs. The gas fraction is constrained to be at least 40%. So far we have only detected a handful of DSFGs at $z > 5$, only a few hundred million years from the Big Bang (Capak et al. 2011; Combes et al. 2012; Walter et al. 2012; Riechers et al. 2013; Strandet et al. 2016). These sources are expected to harbor larger gas reservoirs available for star formation and be able to sustain a more elevated star-formation efficiency than typical DSFGs (Béthermin et al. 2015). Gas fractions of SPT DSFGs derived using low-J CO observations are in the range of 0.3–0.8 (Aravena et al. 2016). Bothwell et al. (2016) found that SPT DSFGs (SPT0346-52 is not in this sample) on average have very high gas fractions ($f_{\rm gas} \sim 0.6$–0.8) based on atomic carbon observations. The very high gas fractions could raise the $\Sigma_{\rm SFR}$ without invoking extremely high star-formation efficiency.

Emission from SPT0346-52 has proved to be beyond the reach of our existing *HST* and *Spitzer* data (Ma et al. 2015),

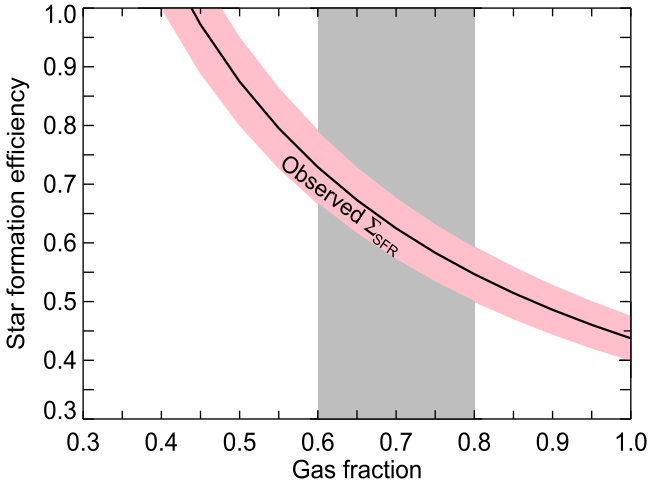

Figure 5. Theoretical expectations based on "maximum starbursts" for the star formation efficiency and gas fraction of SPT0346-52. Very high gas fraction and star-formation efficiency are required to explain the observed $\Sigma_{\rm SFR}$ (the solid line and pink band). The gray band shows the average gas fractions of SPT DSFGs derived from CI observations found by Bothwell et al. (2016).

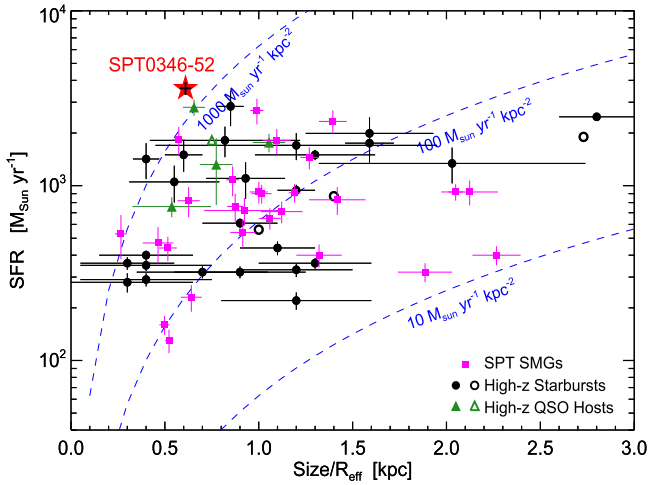

Figure 6. Star formation as a function of dust continuum size for high-redshift dusty starburst galaxies, illustrating that SPT0346-52 (red star with the cross error bar) has an exceptionally large SFR surface density. The dashed lines show constant $\Sigma_{\rm SFR}$ values. The magenta squares are SPT SMGs from Spilker et al. (2016). The black circles are literature starburst galaxies at $z > 3$ with dust continuum size measurements. The green triangles are quasar host galaxies. The open circles and triangles do not have reported error bars. The literature galaxies are drawn from Younger et al. (2008), Walter et al. (2009), Magdis et al. (2011), Walter et al. (2012), Fu et al. (2012), Bussmann et al. (2013), Carniani et al. (2013), Wang et al. (2013a), Cooray et al. (2014), De Breuck et al. (2014), Riechers et al. (2014), Yun et al. (2015), Simpson et al. (2015), and Ikarashi et al. (2015). SFR is based upon $L_{\rm IR}$. $L_{\rm FIR}$ is converted to $L_{\rm IR}$ by multiplying 1.65 when necessary.

[20] To derive the SFR surface density, we divide the SFR by $2\pi R_{\rm eff}^2$ where the factor of 2 corresponds to the half-light radius $R_{\rm eff}$ from the dust emission.

which has prevented a detailed characterization of the established stellar mass. Thus, SPT0346-52 would be an ideal object for follow-up observations with *JWST*.

In this paper we presented a pilot X-ray observation of a single extreme star-forming galaxy at high redshift with *Chandra*. Studying a sample of such vigorously star-forming galaxies in the early universe will help us constrain the formation and co-evolution of the massive galaxies and SMBHs.

We thank the anonymous referee for insightful and constructive comments, which have significantly improved the paper. The scientific results reported in this article are based on observations made by the *Chandra* X-ray Observatory and the Australia Telescope Compact Array. This research has made use of software provided by the *Chandra* X-ray Center (CXC) in the application packages CIAO and Sherpa. The Australia Telescope Compact Array is part of the Australia Telescope National Facility which is funded by the Australian Government for operation as a National Facility managed by CSIRO. The associated *HST*, *Spitzer*, and ALMA data are from PID12659, PID10094, and PID2011.0.00958.S, respectively. This paper makes use of the following ALMA data: ADS/JAO.ALMA #2011.0.00958.S. ALMA is a partnership of ESO (representing its member states), NSF (USA) and NINS (Japan), together with NRC (Canada), NSC and ASIAA (Taiwan), and KASI (Republic of Korea), in cooperation with the Republic of Chile. The Joint ALMA Observatory is operated by ESO, AUI/NRAO and NAOJ.

We acknowledge support from the *Chandra* grant GO5-16116A and the U.S. National Science Foundation under grant No. AST-1312950. M.A. acknowledges partial support from FONDECYT through grant 1140099. Y.H. acknowledges support from Hubble Fellowship grant 51358.001-A awarded by the Space Telescope Science Institute. This research has made use of NASA's Astrophysics Data System.

REFERENCES

Alexander, D. M., Bauer, F. E., Chapman, S. C., et al. 2005, ApJ, 632, 736
Alexander, D. M., & Hickox, R. C. 2012, NewAR, 56, 93
Aravena, M., Murphy, E. J., Aguirre, J. E., et al. 2013, MNRAS, 433, 498
Aravena, M., Spilker, J. S., Bethermin, M., et al. 2016, MNRAS, 457, 4406
Barcos-Muñoz, L., Leroy, A. K., Evans, A. S., et al. 2015, ApJ, 799, 10
Béthermin, M., Daddi, E., Magdis, G., et al. 2015, A&A, 573, A113
Bock, D. C.-J., Large, M. I., & Sadler, E. M. 1999, AJ, 117, 1578
Bothwell, M. A., Maiolino, R., Cicone, C., Peng, Y., & Wagg, J. 2016, A&A, 595, A48
Bradford, C. M., Bolatto, A. D., Maloney, P. R., et al. 2011, ApJL, 741, L37
Bruzual, G., & Charlot, S. 2003, MNRAS, 344, 1000
Bussmann, R. S., Pérez-Fournon, I., Amber, S., et al. 2013, ApJ, 779, 25
Capak, P. L., Riechers, D., Scoville, N. Z., et al. 2011, Natur, 470, 233
Carniani, S., Marconi, A., Biggs, A., et al. 2013, A&A, 559, A29
Chabrier, G. 2003, ApJL, 586, L133
Combes, F., Rex, M., Rawle, T. D., et al. 2012, A&A, 538, L4
Condon, J. J., Cotton, W. D., & Broderick, J. J. 2002, AJ, 124, 675
Cooray, A., Calanog, J., Wardlow, J. L., et al. 2014, ApJ, 790, 40
da Cunha, E., Walter, F., Smail, I. R., et al. 2015, ApJ, 806, 110
Dale, D. A., Helou, G., Magdis, G. E., et al. 2014, ApJ, 784, 83
De Breuck, C., Williams, R. J., Swinbank, M., et al. 2014, A&A, 565, A59
Diamond-Stanic, A. M., Moustakas, J., Tremonti, C. A., et al. 2012, ApJL, 755, L26
Elmegreen, B. G. 1999, ApJ, 517, 103
Elvis, M., Wilkes, B. J., McDowell, J. C., et al. 1994, ApJS, 95, 1
Freeman, P., Doe, S., & Siemiginowska, A. 2001, Proc. SPIE, 4477, 76
Fritz, J., Franceschini, A., & Hatziminaoglou, E. 2006, MNRAS, 366, 767
Fu, H., Yan, L., Myers, A. D., et al. 2012, ApJ, 745, 67
Garmire, G. P., Bautz, M. W., Ford, P. G., Nousek, J. A., & Ricker, G. R., Jr. 2003, Proc. SPIE, 4851, 28
Georgantopoulos, I., Rovilos, E., Xilouris, E. M., Comastri, A., & Akylas, A. 2011, A&A, 526, A86
Gilli, R., Norman, C., Vignali, C., et al. 2014, A&A, 562, A67
Gullberg, B., De Breuck, C., Vieira, J. D., et al. 2015, MNRAS, 449, 2883
Hezaveh, Y. D., Marrone, D. P., Fassnacht, C. D., et al. 2013, ApJ, 767, 132
Hezaveh, Y. D., Marrone, D. P., & Holder, G. P. 2012, ApJ, 761, 20
Hinshaw, G., Larson, D., Komatsu, E., et al. 2013, ApJS, 208, 19
Hodge, J. A., Riechers, D., Decarli, R., et al. 2015, ApJL, 798, L18
Ikarashi, S., Ivison, R. J., Caputi, K. I., et al. 2015, ApJ, 810, 133
Johnson, S. P., Wilson, G. W., Wang, Q. D., et al. 2013, MNRAS, 431, 662
Kennicutt, R. C., Jr. 1998, ARA&A, 36, 189
Laird, E. S., Nandra, K., Pope, A., & Scott, D. 2010, MNRAS, 401, 2763
Lanzuisi, G., Ponti, G., Salvato, M., et al. 2014, ApJ, 781, 105
Lehmer, B. D., Alexander, D. M., Bauer, F. E., et al. 2010, ApJ, 724, 559
Ma, J., Gonzalez, A. H., Spilker, J. S., et al. 2015, ApJ, 812, 88
Magdis, G. E., Daddi, E., Elbaz, D., et al. 2011, ApJL, 740, L15
Martin, C. L. 2005, ApJ, 621, 227
Morić, I., Smolčić, V., Kimball, A., et al. 2010, ApJ, 724, 779
Murphy, E. J., Chary, R.-R., Alexander, D. M., et al. 2009, ApJ, 698, 1380
Murray, N., Quataert, E., & Thompson, T. A. 2005, ApJ, 618, 569
Neri, R., Downes, D., Cox, P., & Walter, F. 2014, A&A, 562, A35
Pacifici, C., Kassin, S. A., Weiner, B., Charlot, S., & Gardner, J. P. 2013, ApJL, 762, L15
Persic, M., & Rephaeli, Y. 2007, A&A, 463, 481
Ranalli, P., Comastri, A., & Setti, G. 2003, A&A, 399, 39
Riechers, D. A., Bradford, C. M., Clements, D. L., et al. 2013, Natur, 496, 329
Riechers, D. A., Carilli, C. L., Capak, P. L., et al. 2014, ApJ, 796, 84
Roehlly, Y., Burgarella, D., Buat, V., et al. 2014, in in ASP Conf. Ser. 485, Astronomical Data Analysis Software and Systems XXIII, ed. N. Manset & P. Forshay (San Francisco, CA: ASP), 347
Rujopakarn, W., Rieke, G. H., Eisenstein, D. J., & Juneau, S. 2011, ApJ, 726, 93
Rush, B., Malkan, M. A., & Edelson, R. A. 1996a, ApJ, 473, 130
Rush, B., Malkan, M. A., Fink, H. H., & Voges, W. 1996b, ApJ, 471, 190
Sargsyan, L., Samsonyan, A., Lebouteiller, V., et al. 2014, ApJ, 790, 15
Simha, V., Weinberg, D. H., Conroy, C., et al. 2014, arXiv:1404.0402
Simpson, J. M., Smail, I., Swinbank, A. M., et al. 2015, ApJ, 807, 128
Spilker, J., Marrone, D., Aravena, M., et al. 2016, ApJ, 826, 112
Spilker, J. S., Aravena, M., Marrone, D. P., et al. 2015, ApJ, 811, 124
Spoon, H. W. W., Farrah, D., Lebouteiller, V., et al. 2013, ApJ, 775, 127
Stacey, G. J., Hailey-Dunsheath, S., Ferkinhoff, C., et al. 2010, ApJ, 724, 957
Strandet, M. L., Weiß, A., Vieira, J. D., et al. 2016, ApJ, 822, 80
Tacconi, L. J., Neri, R., Chapman, S. C., et al. 2006, ApJ, 640, 228
Thompson, T. A., Quataert, E., & Murray, N. 2005, ApJ, 630, 167
Veilleux, S., Meléndez, M., Sturm, E., et al. 2013, ApJ, 776, 27
Vieira, J. D., Crawford, T. M., Switzer, E. R., et al. 2010, ApJ, 719, 763
Walter, F., Decarli, R., Carilli, C., et al. 2012, Natur, 486, 233
Walter, F., Riechers, D., Cox, P., et al. 2009, Natur, 457, 699
Wang, R., Wagg, J., Carilli, C. L., et al. 2013a, ApJ, 773, 44
Wang, S. X., Brandt, W. N., Luo, B., et al. 2013b, ApJ, 778, 179
Weiß, A., De Breuck, C., Marrone, D. P., et al. 2013, ApJ, 767, 88
Xue, Y. Q., Luo, B., Brandt, W. N., et al. 2011, ApJS, 195, 10
Younger, J. D., Fazio, G. G., Wilner, D. J., et al. 2008, ApJ, 688, 59
Yun, M. S., Aretxaga, I., Gurwell, M. A., et al. 2015, MNRAS, 454, 3485
Yun, M. S., Reddy, N. A., & Condon, J. J. 2001, ApJ, 554, 803